Effect of Processing Parameters on Microstructure and Mechanical Properties of Al6061/B_4C Metal Matrix Composite Fabricated by Using Stir Casting, Post-Accumulative Roll Bonding and Aging Treatment

Y. Pazhuhanfar & B. Eghbali

Transactions of the Indian Institute of Metals

ISSN 0972-2815

Trans Indian Inst Met
DOI 10.1007/s12666-018-1506-6

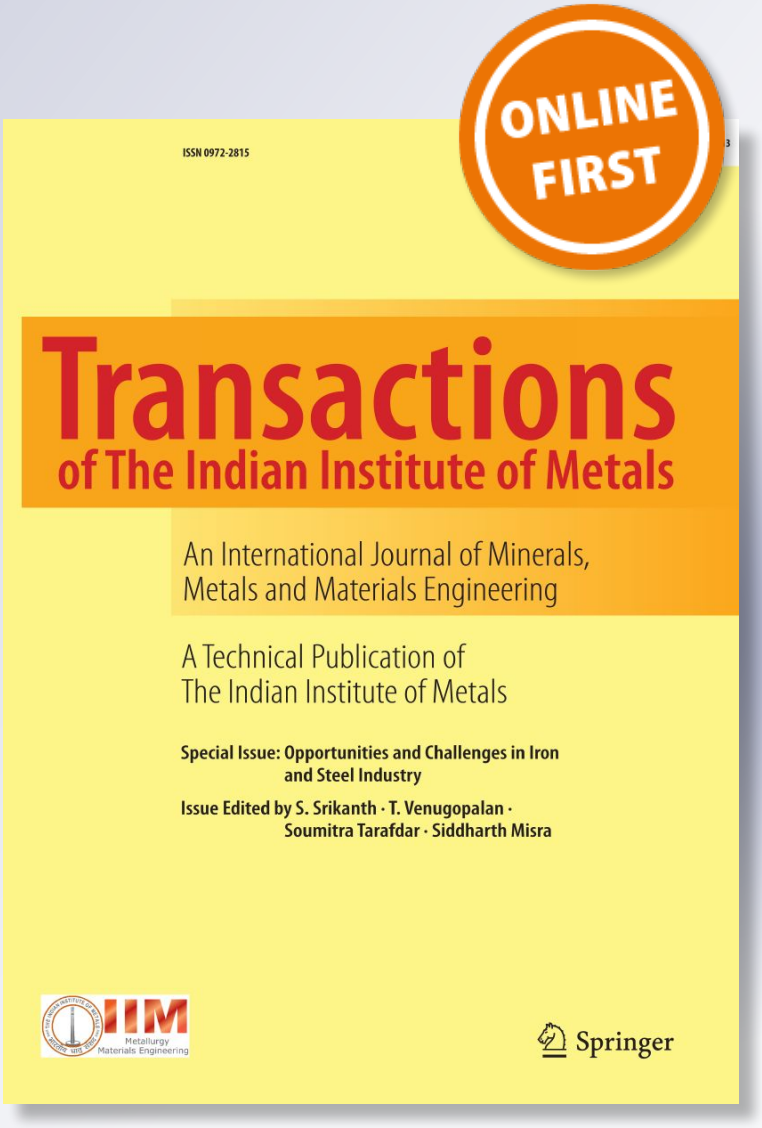

Springer

Trans Indian Inst Met
https://doi.org/10.1007/s12666-018-1506-6

TECHNICAL PAPER

Effect of Processing Parameters on Microstructure and Mechanical Properties of Al6061/B_4C Metal Matrix Composite Fabricated by Using Stir Casting, Post-Accumulative Roll Bonding and Aging Treatment

Y. Pazhuhanfar[1] · B. Eghbali[1]

Received: 15 January 2018 / Accepted: 5 November 2018

Abstract In the present research, Al6061-based composites reinforced with micron-sized B_4C particles were fabricated by the combination of stir casting and post-processing via accumulative roll bonding (ARB) and aging treatment. Microstructural evolutions of processed samples were investigated using optical and scanning electron microscopy. Also, mechanical properties were studied by micro-hardness measurements and room temperature tensile testing. From obtained results, it was concluded that the as-cast composites had a lower tensile strength and elongation compared with accumulative roll-bonded counterparts. Post-processing by accumulated roll bonding decreased the deficiencies aroused during stir casting and improved particle distribution. It was observed that increasing ARB cycles decreased the particle-free zones and particle clusters.

Keywords Al6061–B_4C composite · Stir casting · Accumulative roll bonding · Aging treatment

1 Introduction

Accumulative roll bonding (ARB) is a severe plastic deformation method proposed by Saito et al. [1] for production of ultrafine grained and nanostructured metallic materials [2–4]. So far, ARB technique has been extensively used for improvement of the strength of metals and alloys through microstructure refinement [5–7]. Also, tremendous researches have been conducted on the fabrication of particulate reinforced metal matrix composites by adding ceramic particles between metallic sheets before rolling [8–10]. It has been found that the tensile strength and hardness can be improved in MMCs produced by accumulative roll bonding but considerable decrease in elongation and ductility is observed [11]. This decrease in ductility has been attributed to different factors such as increased dislocation density in matrix material and the impaired bonding between ceramic particles and matrix material, which occurs in solid state under the pressure of rollers, due to the presence of contaminations [12]. Among MMCs, aluminum and aluminum alloys have a considerable application as matrix material due to the processing flexibility, low melting point, low density, high corrosion resistance and heat treatment capabilities [13–15]. Aluminum matrix composites are fabricated by incorporating a variety of ceramic particles such as B_4C [16], Al_2O_3 [17], TiB_2 [18], SiC [19] into a matrix using different processing techniques. Among different ceramic particles, boron carbide (B_4C) has great advantages such as lower density compared to aluminum and higher stiffness and hardness. Meanwhile, the nuclear properties of boron carbide like high neutron absorption capacity and resistance to irradiation have made it an attractive choice for production of nuclear power plant parts [20, 21]. In the present work, Al6061 alloy was used as matrix material due to its optimum combination of strength and ductility among different aluminum alloys. Stir casting was then used for production of Al6061–B_4C composites and accumulative roll bonding and aging treatment was employed as post-processing to improve mechanical properties by increasing the uniformity of the reinforcement distribution and other mechanisms. Improving the bonding strength of particles and matrix alloy can be achieved provided that the sufficient

✉ B. Eghbali
eghbali@sut.ac.ir

[1] Department of Materials Science and Engineering, Sahand University of Technology, Tabriz, Iran

Published online: 20 November 2018

wettability of ceramic particles is obtained by adding titanium or other compounds such as K_2TiF_6 into the melt [22]. In this work, fabricated composites were subjected to accumulative roll bonding up to five cycles and their microstructures and mechanical properties were evaluated. Results indicate that the combination of stir casting, accumulative roll bonding and aging treatment is a promising route for the production of AMCs with high strength and sufficient ductility.

2 Material and Experimental Procedure

Al6061 alloy was used as matrix material, and B_4C ceramic powders with an average size lower than 10 μm were used as reinforcement phase. The chemical composition of Al6061 alloy is represented in Table 1. Also, the SEM micrograph and X-ray diffraction pattern of B_4C particles are illustrated in Fig. 1. Al6061 matrix composites with 3, 6 and 9 wt% B_4C were fabricated using stir casting method. These samples were nominated as 0, B3, B6 and B9, respectively. For this reason, 0.5 kg of Al6061 alloy was melted in a ceramic crucible with a capacity of 1 kg. At first, B_4C reinforcement particles were mixed with K_2TiF_6 for 1.5 h in tubular mixer and then preheated in electric furnace at 250 °C for 2 h. The furnace temperature of stir casting machine was set to 700 °C and the melt was kept at this temperature for 5 min to achieve uniform temperature through the melt. Afterward, molten Al6061 alloy was stirred at 350 rpm for 15 min using impeller made of titanium, and preheated powders were injected into the vortex under argon atmosphere. After injection of reinforcements, the melt was poured immediately into a permanent die made of steel with dimensions of 170 × 60 × 20 mm. Casted slabs were cut into plates and each plate was cold rolled to the thickness of 1 mm. In the first ARB cycle, four as-rolled plates were stacked over each other after surface preparation and rolled to a thickness of 1 mm. In the second ARB pass, three plates were stacked over each other and rolled to the thinness of 1 mm. The process of cutting, surface preparation, stacking and roll bonding were repeated up to five cycles. After five cycles of roll bonding, the number of layers reached to 324. The schematic representation of this process is illustrated in Fig. 2a and the stacked and roll-bonded plates are shown in Fig. 2b. Samples were then solution treated at 540 °C for 1.5 h. Two-step aging treatment was conducted at 130 °C for 2 h and at 190 °C for 4 h. The microstructure of stir-casted, roll-bonded and age-treated composites was analyzed after each cycle using optical and scanning electron microscopy. For this reason, samples were mounted and the selected surfaces were prepared using sandpapers with different grits of 100–5000 and then mechanically polished by Al_2O_3 suspension. Optical micrographs were taken before and after etching by the use of Olympus PMG3 microscope and SEM images were acquired using Tescan MIRA3 scanning electron microscope. In order to determine the percentage of residual porosity in the specimens, at first the bulk density and then the relative density was calculated based on the relationships 1–3, through the Archimedes method. The steps of measuring the density are: (1) dry weight (Wair) was measured, (2) The sample was suspended in distilled water and its weight (Water) was measured, (3) Finally, the bulk density, the theoretical density and the relative density were calculated based on the following relationships.

Table 1 Chemical composition of as-cast Al6061 alloy

Element	Al	Mg	Si	Fe	Cu	Cr	Ti	Mn	Zn
Content (wt%)	97.31	1.21	0.58	0.31	0.26	0.21	0.03	0.02	0.01

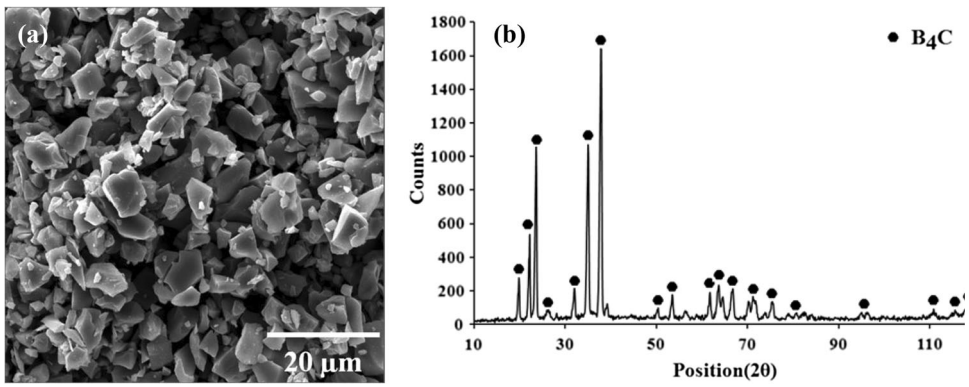

Fig. 1 aSEM micrograph, **b** X-ray diffraction pattern of B_4C reinforcement particles

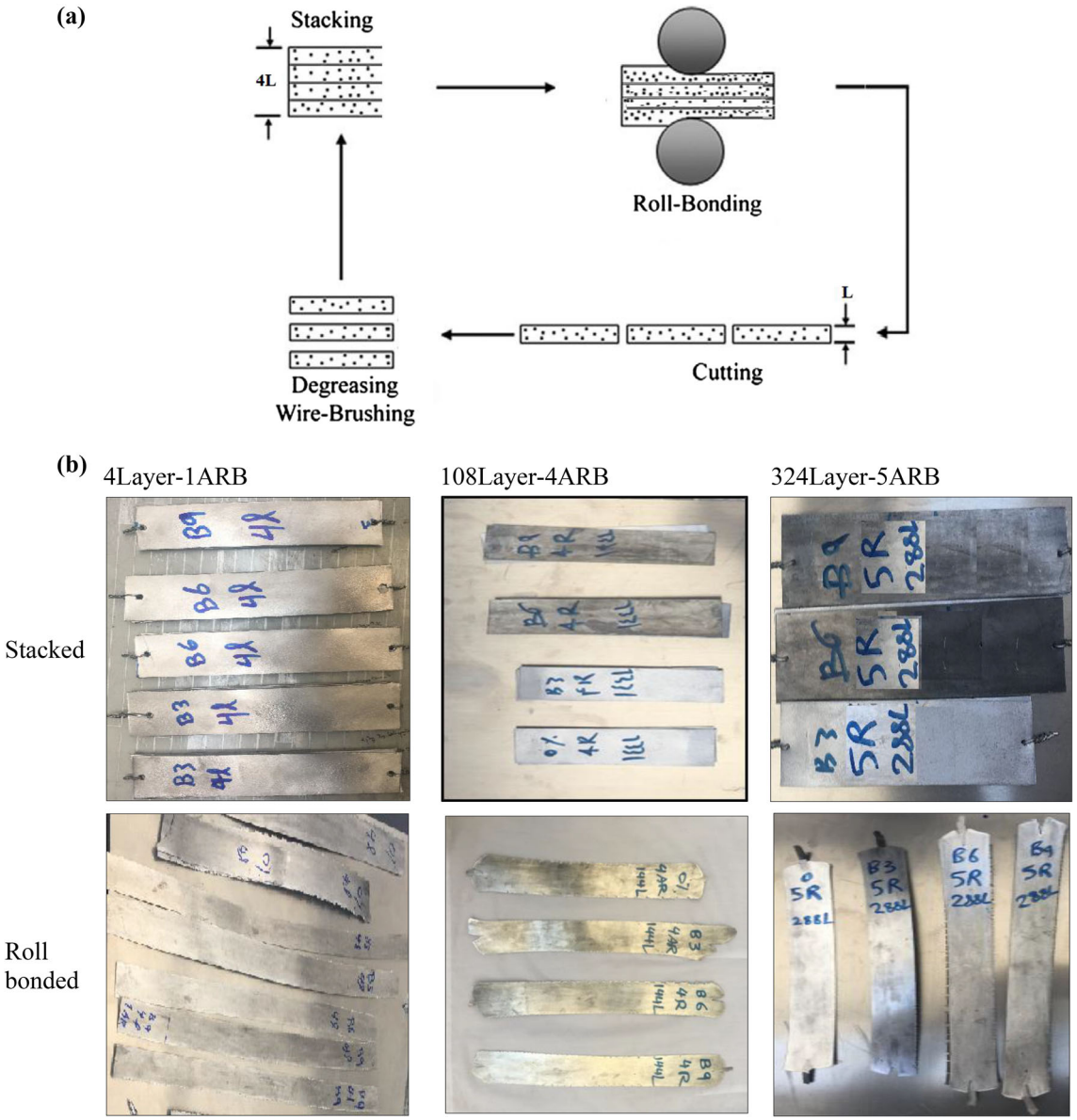

Fig. 2 aSchematic representation of ARB process, **b** stacked and roll-bonded plates

Indeed, the theoretical density was determined using the mixing rule and according to the density of each of the constituent elements of the composition. Subsequently, the relative density was calculated from the ratio of the bulk density to the theoretical density.

$$\rho_b = \frac{\text{Wair}}{\text{Wair} - \text{Wwater}}$$

$$\frac{1}{\rho_t} = \sum_{i=1}^{N} \frac{\text{wt\%}_i}{\rho_i}$$

$$\rho_r = \frac{\rho_b}{\rho_t} \times 100$$

where ρ_b is bulk density, ρ_t is the theoretical density of the sample, wt% is the weight percentage of each element, ρ_i is the density of each element and ρ_r is relative density. Finally, the porosity percentage of the specimen is calculated from the following equation.

$$\%\text{porosity} = 100 - \rho_r$$

Tensile tests were conducted at room temperature in order to evaluate mechanical properties of the casted, roll-bonded and age-hardened composites. Tensile samples were prepared according to ASTM E8M standard, respectively. Tensile tests were conducted with the rate of 1 mm/min using GOTECH Al-7000-LA 10 testing machine. Also, micro-hardness of samples was measured by applying 25 g load for 10 s.

3 Results and Discussions

3.1 Microstructure Observation

Figure 3 shows optical microstructures of Al6061 matrix alloy at different conditions. Figure 3a and b represent the as-cast microstructures at different magnifications. As it is clear, the microstructure consists of α matrix and Mg_2Si precipitates and Al–Si–Mg ternary eutectic at grain boundaries. Figure 3c shows the microstructure after rolling. In this micrograph, α grain is observed to be elongated in the rolling direction. Also, Mg_2Si precipitates are distributed at grain boundaries which are aligned parallel to rolling direction. Microstructure after aging treatment is shown in Fig. 3d. As can be seen in this figure, grains became equiaxed due to the occurrence of static

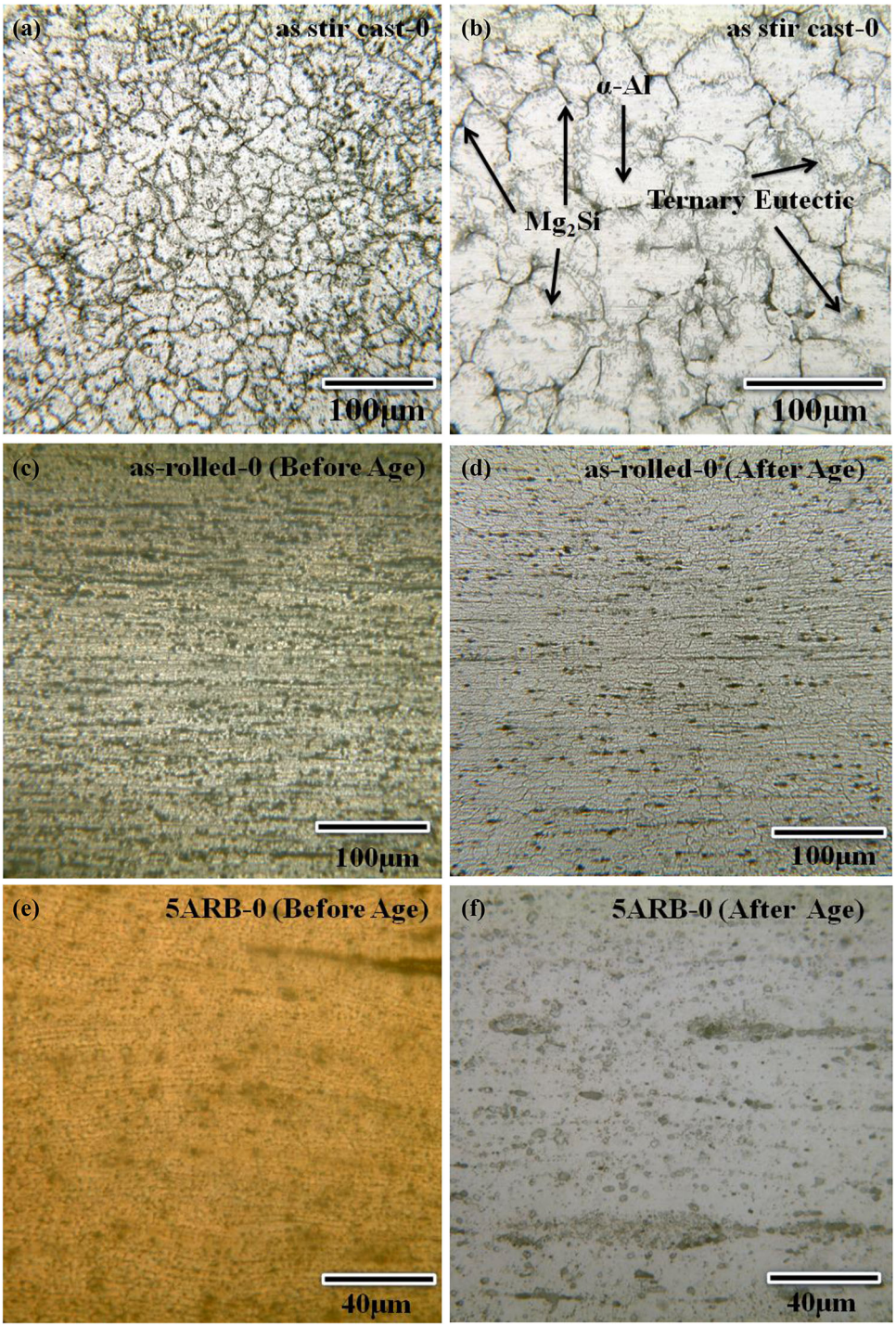

Fig. 3 Optical microstructures of Al6061 matrix alloy at different conditions: **a**, **b** as stir casted, **c** as rolled (before aging), **d** as rolled (after aging), **e** 5ARB (before aging), **f** 5ARB (after aging)

recrystallization during solution treatment at 540 °C. Also, Mg_2Si precipitates are distributed more uniformly than as-rolled condition (Fig. 3c). Figure 3e shows microstructure of Al6061 matrix after 5ARB cycles. It is obvious that the grain structure is more refined compared with as-rolled condition and Mg_2Si precipitates are finer. Also after aging treatment (Fig. 3f), a more uniform microstructure with finer Mg_2Si precipitates compared with as-rolled condition (Fig. 3d) is developed. Figure 4 represents FE-SEM micrographs from Al6061 matrix alloy at different processing conditions. The stir-casted microstructure is shown in Fig. 4a. As can be seen, Mg_2Si precipitates are distinctive as layers at α grain boundary. Also, a higher magnification of Al–Si–Mg ternary eutectic region is represented in Fig. 4b. Figure 4c shows microstructure after rolling of as-cast samples. In this figure, matrix phase is shown as

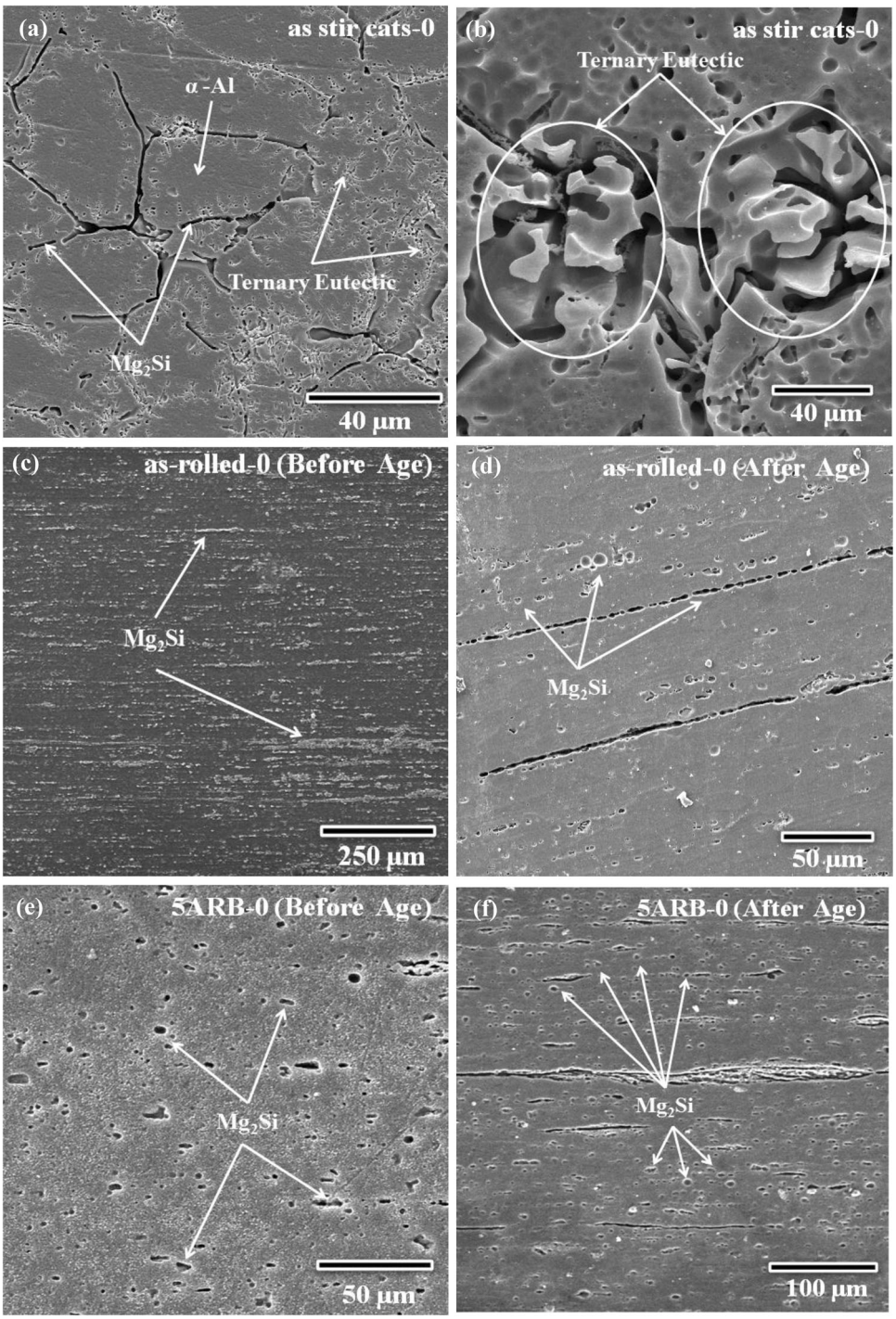

Fig. 4 SEM micrographs of Al6061 matrix alloy at different conditions: **a**, **b** as stir casted, **c** as rolled (before aging), **d** as rolled (after aging), **e** 5ARB (before aging), **f** 5ARB (after aging)

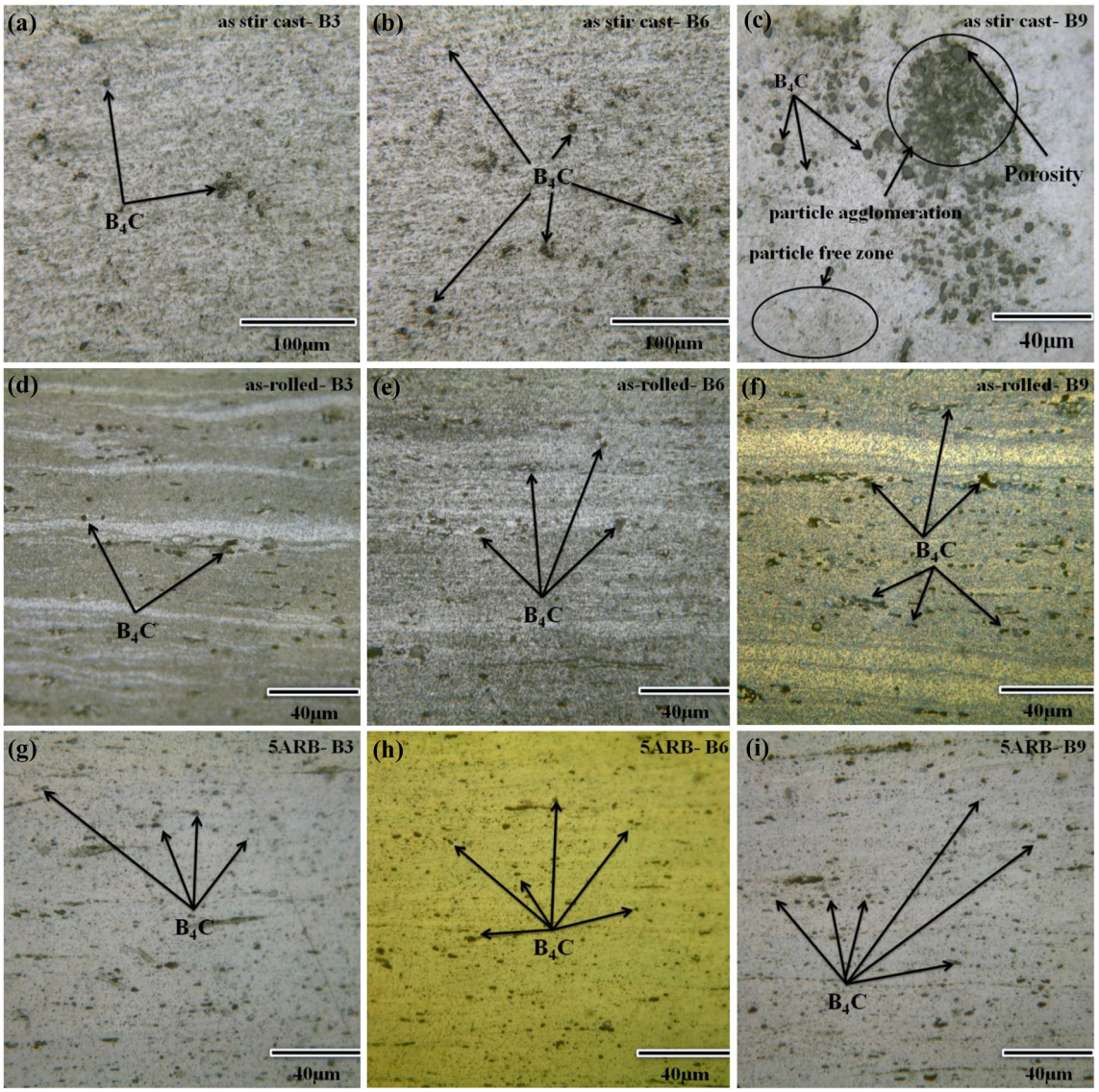

Fig. 5 Optical microstructures of Al6061-B_4C composites at different conditions: **a–c** as stir casted, **d–f** after rolling, and **g–i** after 5ARB

dark area and Mg_2Si precipitates are represented as bright gray phase distributed linearly on primary α phase boundaries which are aligned parallel to rolling direction. But after aging treatment of as-rolled Al6061 matrix alloy, static recrystallization of matrix followed by precipitation of Mg_2Si phase results in more uniform distribution of precipitates at the interior and boundaries of α phase (Fig. 4d). Comparing Fig. 4c and d, it can be said that the Mg_2Si distribution becomes more uniform with solutionizing and aging treatment. Figure 4d shows the microstructure after 5ARB cycles. As it is evident, the distribution of Mg_2Si precipitates is more uniform compared with as cast (Fig. 4a) and as-rolled samples (Fig. 4c). Also, particle-free zones existing mostly at grain interiors are eliminated after rolling by imposing severe plastic deformation using accumulative roll bonding (compare Fig. 4c with e). Also, the most uniform distribution of fine Mg_2Si precipitates is achieved by aging treatment of roll-bonded Al6061 matrix alloy (Fig. 4f). Figure 5 represents the distribution of B_4C reinforcement particles in Al6061–B_4C composites at different processing conditions. In the case of Al6061–3 wt% B_4C composite (Fig. 5a), reinforcement particles are distributed non-uniformly in matrix. Also, some agglomerated particles are observed in conjunction with particle-free zones with the increase in reinforcement fraction to 6 wt% (Fig. 5b). Comparing the stir-casted microstructures of composites with different fractions of reinforcement, it is concluded that the most non-uniform microstructure is achieved by incorporation of 9 wt% B_4C in Al6061 matrix (Fig. 5c). There are some clusters and particle-free zones that affect mechanical properties adversely. Degradation of mechanical properties

at as stir cast condition is also due to the existence of stress concentrations and porosities at cluster regions (Fig. 5c) where there is not enough bonding between the cluster and matrix material. It seems that the high level of surface energy around B_4C particles and the possibility of adherence of particles together during the casting process have prevented their uniform distribution. In fact, in samples containing low amount of B_4C, the presence of K_2TiF_6 has been able to play its role as an agent that enhances the wettability, reduce the surface energy of the Al/B_4C interfaces and create a good bond between aluminum and boron carbide. While in the B9-C sample, the non-uniform distribution of particles during casting and the near impossibility of affecting the K_2TiF_6 phase on all reinforcement particles reduces the wettability and results in air gap between the B_4C and the aluminum matrix.

The reaction between B_4C and aluminum in the region of the Al/B_4C interface can be done as follows [23–26]:

$$9Al + 2B_4C = 2Al_3BC + 3AlB_2$$

This reaction results in the formation of Al_3BC and AlB_2 phases. Also, by adding the K_2TiF_6 to the liquid aluminum containing B_4C particles, each of the components individually has effects on the Al matrix and the reinforcing particles. According to the investigation carried out by researchers, there are several reactions that can show how K_2TiF_6 decomposes in aluminum, some of which include [23–26]:

$$18K_2TiF_6 + 24Al = 6(3KF \cdot AlF_3) + 18(KF \cdot AlF_3) + 18Ti$$
$$K_2TiF_6 = 2KF + TiF_4$$
$$3K_2TiF_6 + 13Al = 3Al_3Ti + 3KAlF_4 + K_3AlF_6$$

As can be seen, the phases produced as a result of the reaction between K_2TiF_6 and Al can include KF, AlF_3, TiF_4, AlF and Al_3Ti. Also, since before the addition of B_4C and K_2TiF_6 to aluminum, the mixture of powder was first subjected to preheat operation at 250 °C, there is the probability of formation of boron oxide on the surface of the B_4C and titanium oxide on the surface of K_2TiF_6. Thus, there is the possibility of the occurrence of each of the two following reactions and formation of AlB_2 and Al_3Ti phases [23–26]:

$$3AL + B_2O_3 = Al_2O_3 + AlB_2$$
$$13Al + 3TiO_2 = 2Al_2O_3 + 3Al_3Ti$$

Subsequently, two new products (AlB_2 and Al_3Ti) can react with each other again and lead to the formation of TiB_2 [23–26]:

$$AlB_2 + Al_3Ti = 4Al + TiB_2$$

However, due to the presence of K_2TiF_6 and B_4C particles in aluminum, the TiC phase will not be formed in the Al matrix. On the whole, despite the addition of K_2TiF_6 to aluminum, the formation of brittle phases (AlB_2 and Al_3Ti) in the matrix has reduced the strength. Rolling of composites after stir casting process significantly affects the distribution of reinforcement particles in matrix. Figures 3f to 5d show the microstructure of composites after rolling step. It is evident that the uniformity of particles distribution is improved by rolling. As shown in Fig. 5d and e, particle's distribution in Al6061–B_4C composites with 3 and 6 wt% B_4C is almost uniform, after rolling. But the microstructure of Al6061–9 wt% B_4C composite is still non-uniform and consists of particle-free zones and clusters but its uniformity is improved compared with stir-casted condition (Fig. 5f). The optical microstructures of Al6061–B_4C composites at the final stage after imposing fifth cycles of ARB are shown in Fig. 5g–i representing an appropriate distribution of reinforcement particles in the matrix without agglomeration. Different factors have an influence on particle's distribution during deformation with accumulative roll bonding. For example, shear bands are formed at matrix and reinforcement interface by imposing plastic strain through ARB process. Shear bands move within the matrix and break into clusters leading to displacement of reinforcement particles and improvement in their distribution in matrix [27]. It has also been demonstrated that the stacking fault energy of matrix material has an influence on the particle distribution. By increasing SFE, the formability of matrix material becomes easier and the rate of particle distribution is increased [28]. Deformation temperature is another factor influencing the particles distribution. As the temperature increases, more sliding systems are activated and dislocation climb and cross-slip occur more easily and these factors lead to the separation, movement and distribution of particles in matrix [29]. Also, the reinforcing particle size has an influence on the achievement of uniform particle distribution. It has been shown that the composite with larger reinforcing particles achieves a more uniform distribution compared to composite with smaller reinforcing particles [30]. Accumulative roll bonding not only improves the particle distribution within matrix but also increases the bonding strength between the particle and matrix and further results in grain refinement of matrix materials. FE-SEM micrographs from microstructures of Al6061–9 wt% B_4C composite are shown in Fig. 6 for more detailed analysis of the particle/matrix interface. As shown in Fig. 6a, coarse particle zones exist in the as-rolled condition and micro-cracks are detected in the particle–matrix interface at higher magnifications (Fig. 6b). But after five cycles of accumulative roll bonding, a uniform distribution of fine B_4C particles is achieved (Fig. 6c) and cracks in the

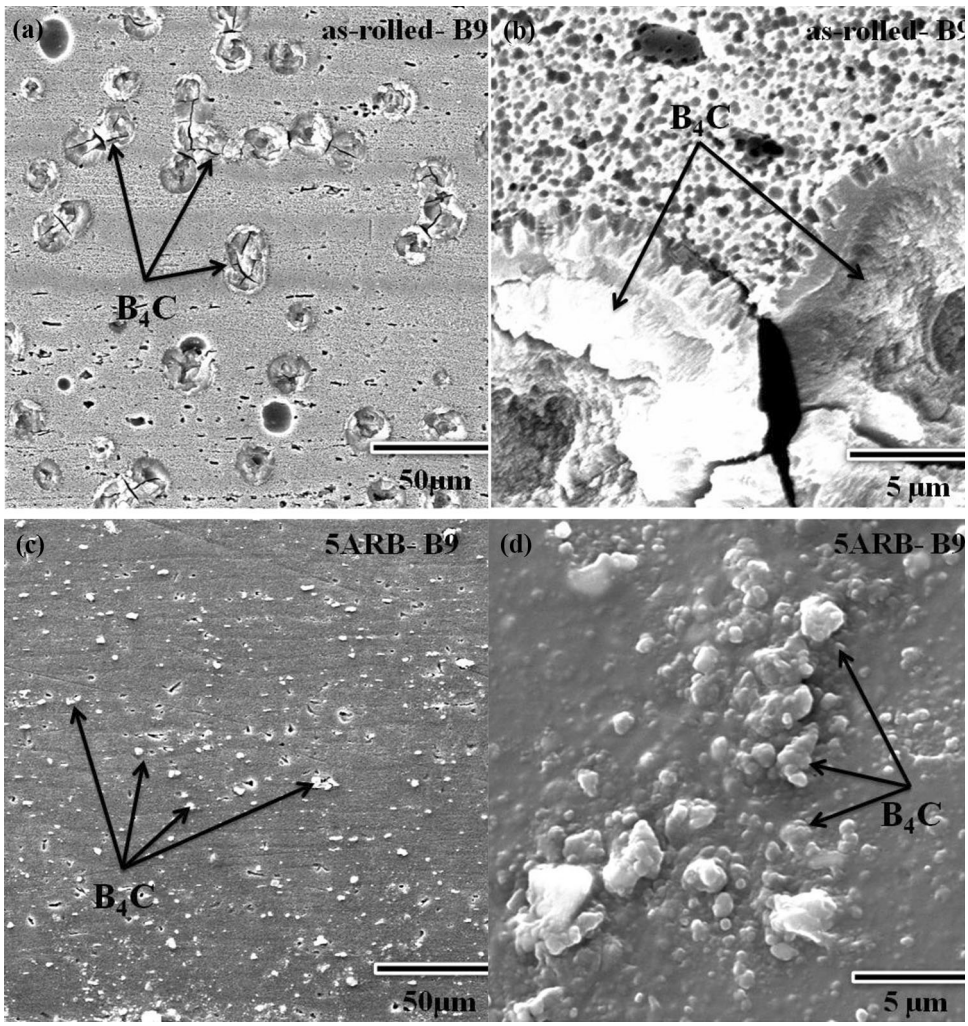

Fig. 6 SEM micrographs showing the particle distribution and interface quality for Al6061–9 wt%. B_4C composite: **a**, **b** as-rolled condition and **c**, **d** after five ARB cycles

particle/matrix interface are eliminated (Fig. 6d) leading to improved mechanical properties which are shown in the next part.

3.2 Mechanical Properties

3.2.1 Tensile Strength and Elongation

Figure 7 shows the variations of tensile strength and elongation of as stir-casted Al–B_4C composites with the volume fraction of reinforcement particles. As it is evident, tensile strength and elongation to failure are both decreased with the increase in reinforcement fraction. The decrease in tensile strength with reinforcement quantity is in contrast with common reports regarding the effect of reinforcement fraction on mechanical properties of composites [31–33]. This discrepancy arises from the lower bonding strength of reinforcement and matrix in fabricated as-cast Al–B_4C composites in the present investigation. It has been proven that the mechanical properties of material can be improved

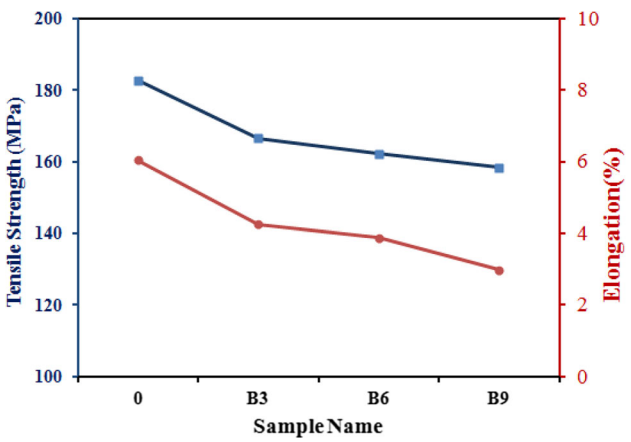

Fig. 7 Variations of tensile strength and elongation of Al–B_4C composites with fraction of reinforcement

with incorporation of ceramic particles provided that the sufficient bonding between matrix metal and reinforcement is established. In this investigation, the low wettability of

B_4C particles with Al melt results in the formation of particle agglomeration and entrapment of air into the matrix and reinforcement interface. Therefore, the load bearing capacity of fabricated composite is decreased. Also, micro-cracks are initiated conveniently at lower tensile stresses due to stress concentrations at particle and matrix interface. These are the main reasons behind degradation of the tensile strength and elongation to failure of Al–B_4C composites produced by stir casting in the present study. Moreover, another effective factor in reducing tensile strength can be the presence of brittle intermetallic phases in the matrix/reinforcement interfacial region and the weak bond between the Aluminum and B_4C particles. In fact, as a result of the in situ reaction between boron carbide and aluminum matrix, a brittle Al_3BC phase is formed that can reduce tensile strength [23, 24]. The tensile stress–strain curves of the processed specimens are shown in Fig. 8. Also, Fig. 9 shows the variations of tensile strength of Al6061–B_4C composites with B_4C contents of 3, 6, and 9 wt% with ARB cycles for before and after aging conditions. As it is seen, mechanical properties are improved with the number of ARB cycles in both before aging and after aging conditions. Regarding before aging condition, it can be said that processing with accumulative roll bonding alters mechanical properties by different mechanisms. One of the main factors is the microstructure evolutions of the matrix material with plastic deformation. At early cycles of ARB process, strain hardening resulting from generation and multiplication of dislocations plays an important role in increasing the tensile strength. With increasing ARB cycles, dislocations are arranged in the form of low energy dislocation walls and are finally converted to low and high angle boundaries. Therefore, at higher ARB cycles, grain refinement is predominant factor that influences mechanical properties. As shown in Fig. 9, tensile strength is increased with steeper slope at early stages of ARB processing due to work hardening. By increasing plastic strain, the rate of increase in tensile strength is decreased where grain refinement plays an important role than strain hardening. It is also evident in Fig. 9 that the tensile strength of fabricated composites is decreased with B_4C content at lower deformation cycles but is improved with increasing B_4C content at higher deformation cycles both at before and after aging conditions. This can be explained by the rule of mixture. As the strength and stiffness of B_4C particles are higher than Al6061 matrix, the tensile strength is improved with the increase in volume fraction of B_4C reinforcement particles. This explanation is true provided higher bonding strength is established between reinforcement and matrix. So, it is concluded that the bonding strength at lower deformation cycle is lower than critical value to improve mechanical properties, but it increases with post-deformation of composites so that the strength is increased with reinforcement fraction at higher ARB cycles (three, four and five cycles). There are some other factors that have influence on the strength and elongation of metal matrix composites reinforced with ceramic particulates. One of the main reasons for lower strength and ductility of as-cast composites (Fig. 7) is the formation of porosities in the microstructure of casted composite material. Porosities exist mainly in the interface of particle agglomerates and matrix. Increasing ARB cycles leads to uniform distribution of reinforcement in matrix and eliminate porosities. So that, the tensile strength and elongation are both improved with ARB processing of as-cast metal matrix composites. The other reason is the difference between thermal expansion coefficients of reinforcement particles and matrix material. Due to this difference, thermal stresses are created in the matrix and the reinforcement intersections. These thermal stresses lead to localized deformation in the matrix material near the particle and matrix intersections. Increased dislocation density due to this phenomenon causes the strength and elongation of composite to decrease. Similar results are shown in case of fabricated composites after aging treatment. As it is seen, the tensile strength of composites after aging treatment is increased with the increase in roll bonding cycles. It should be noted that during solution treatment of composites at 540 °C, static recrystallization occurs in aluminum matrix. As the ARB cycles are increased, the local differences in dislocation density are increased in aluminum matrix and the mean grain size of recrystallized grains is decreased with the increase in ARB cycle. Therefore, the tensile strength of composites after aging treatment is increased with the increase in ARB cycle. It is also evident that the strength of composites is increased with aging treatment (Fig. 9). This is due to the formation of fine dispersed Mg_2Si precipitates as a result of aging treatment. Figure 10 represents the variation of elongation to failure of composites with ARB cycle. As can be seen, in all composites (0, 3, 6 and 9 wt% B_4C), elongation to failure first increases up to one ARB cycle and then decreases with increasing deformation cycles. The increase in elongation during initial stages of deformation is due to the reduction of porosity content and also the improvement of the bonding strength between reinforcement and matrix aluminum alloy. It is also clear that the elongation to failure decreases with ARB cycle with further deformation. This is due to the work hardening and increasing dislocation density in matrix alloy. A similar trend is also observed in the age-hardened condition. Also, it is seen that the elongation to failure increases with aging treatment. This can be attributed to the occurrence of static recrystallization in aluminum matrix during solutionizing.

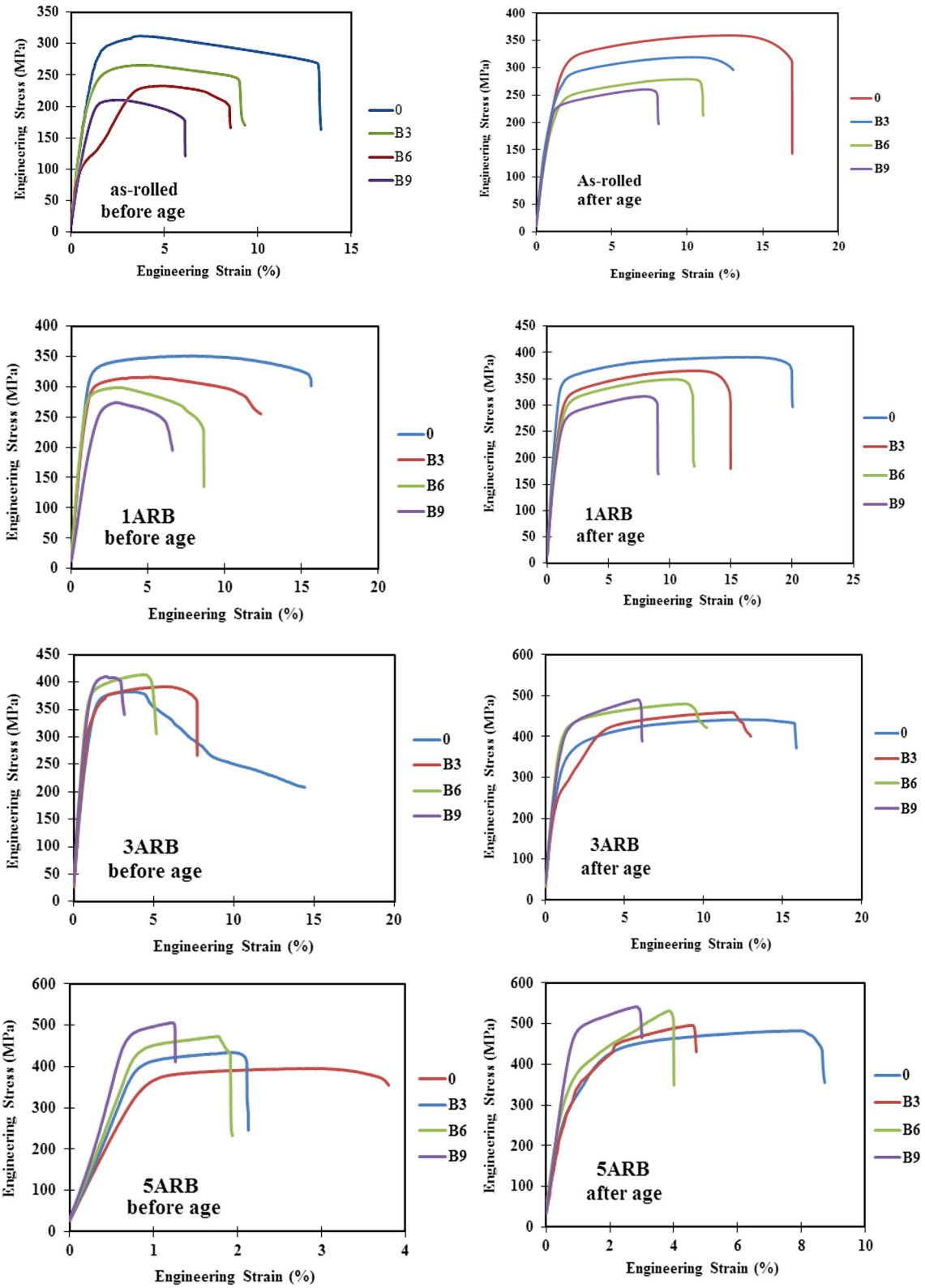

Fig. 8 Engineering tensile stress–strain curves of the processed samples

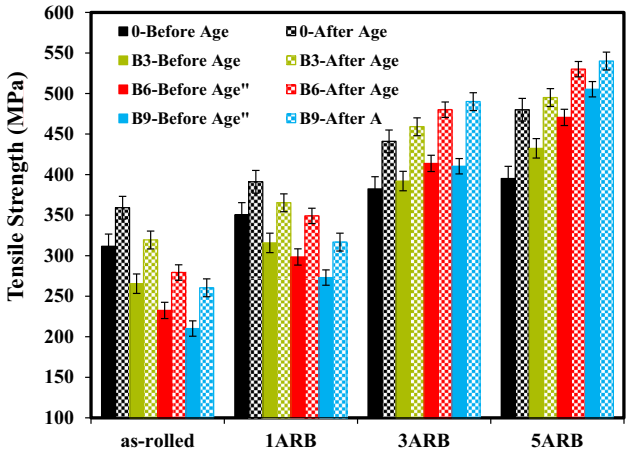

Fig. 9 Variations of the tensile strength of Al–B_4C composites with deformation cycles at two conditions of before and after aging treatment

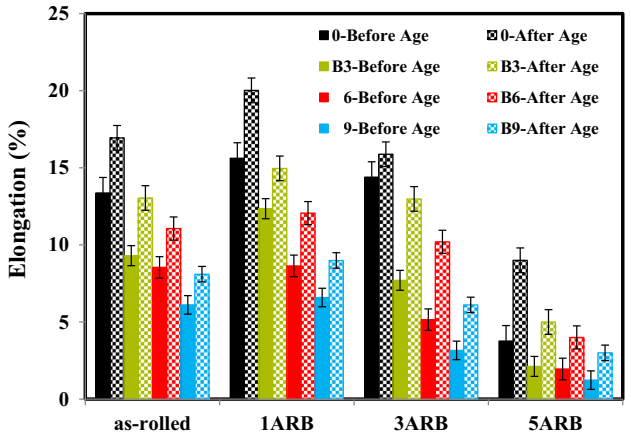

Fig. 10 Variations of the elongation to failure of composites with ARB cycles in both before aging and after aging conditions

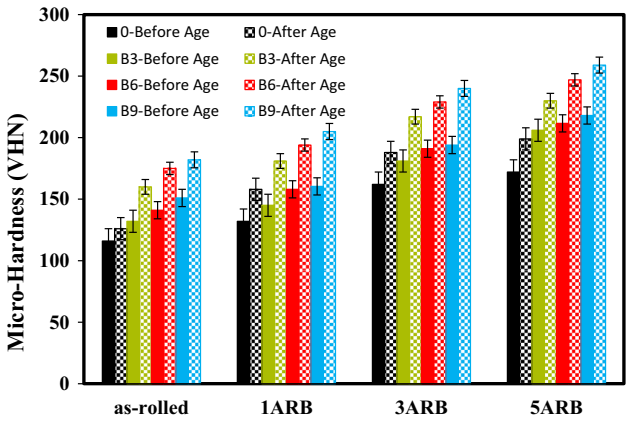

Fig. 11 Variations of the elongation to failure of composites with ARB cycles in both before aging and after aging conditions

3.2.2 Micro-Hardness Measurement

Figure 11 represents the variations in the hardness of fabricated composites with ARB cycles at different reinforcement contents just before and after aging treatment. As can be seen, the micro-hardness of all composites increases with increasing ARB cycles. Rapid increase in hardness at early stages of accumulative roll bonding is due to strain hardening. Generation of dislocations and the formation of dislocation forests at the early stages increase both hardness and strength remarkably. Also, it can be said that due to applications of the highest value of work hardening during severe plastic deformation of metals, saturation in hardness value is obtained which can be observed here in the case of Al6061-B_4C reinforced composite. It is also deduced that hardness value is improved with the increase in the volume fraction of reinforcement. The increased hardness of composite material with respect to non-reinforced matrix material is due to the role of reinforcement particles in hindering dislocation motion by Orowan mechanism. It should be noted that the occurrence dynamic recovery in matrix decreases the strength and hardness of the composite material. At the early stage of accumulative roll bonding, the effect of work hardening is more important than the effect of recovery and a sharp increase in hardness is observed at early cycles. By increasing ARB cycles, the role of recovery in decreasing hardness is more pronounced than early stages. So that, the rate of the increase in hardness slows down with the increase in ARB cycles. Also, increasing the number of ARB passes improves the bonding quality of matrix and reinforcements and also increase the uniformity of the reinforcement distribution in matrix. These two factors make hardness and tensile strength to increase with deformation cycles. The similar trend is also observed in after aging condition. Also, it is observed that the hardness of composites is increased with aging treatment. This is due to the effect of Mg_2Si precipitates formed in matrix Al6061 alloy during T6 aging treatment.

3.3 Porosity Measurement

Figure 12 shows the variation in porosity content of composites with ARB passes for different Al601–B_4C composites. As can be seen, the fraction of porosities decreases with increasing ARB cycles for all composites. Also, the porosity content increases with the increase in reinforcement fraction. This may be due to the reduction of porosity content as a result of decrease in particle clusters. Particle clusters contain some air entrapped during solidification which may be eliminated by imposing plastic deformation. So, it can be said that particle agglomeration leads to porosity formation and the elimination of agglomerates

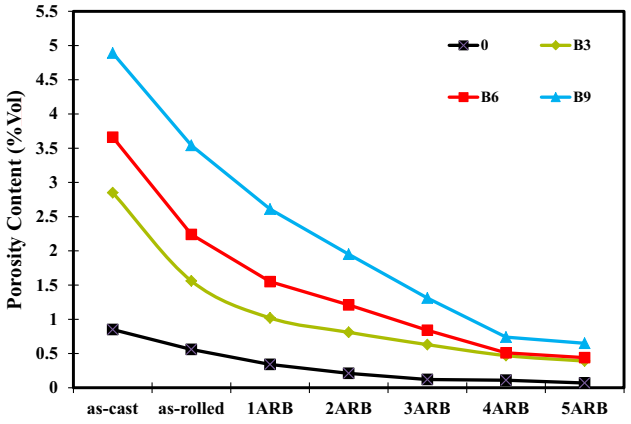

Fig. 12 Variations of the porosity content of composites with ARB cycles

with increasing the amount of plastic deformation causes the porosity content to decrease.

3.4 Fracture Analysis

Figure 13 shows fractured surfaces of Al6061 matrix alloy and Al6061–9 wt% B_4C composite at different conditions. As can be seen, the fractured surface of as-cast Al6061 alloy (Fig. 13a) consists of cleavage facets indicating that cracks are initiated and they propagate through α phase boundaries where the interface between Mg_2Si and matrix provides preferential sites for crack initiation. In case of Al6061–9 wt% B_4C composite in the as-cast state (Fig. 13b), apart from cleavage fracture initiated from grain boundaries, ductile dimples are observed at some regions. These ductile dimples are initiated from particle/matrix interface, and finally, the fracture occurs with growth and coalescence of micro-voids. Figure 13c represents the fracture surface of Al6061 matrix alloy after rolling. It is concluded that brittle fracture is the main cause of failure similar to as-cast condition but the number of initiated cracks increases with plastic deformation. This

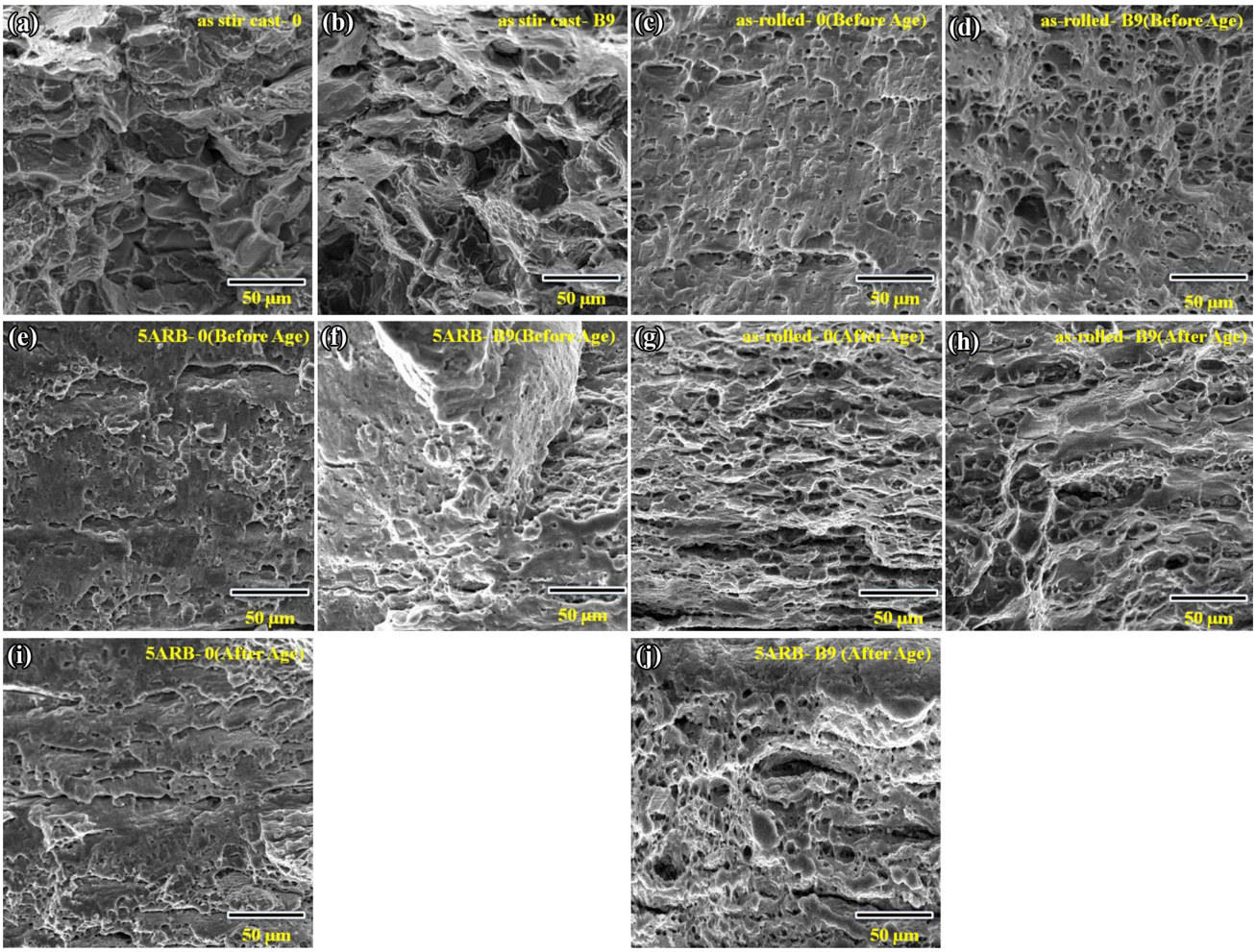

Fig. 13 SEM micrographs from fractured surfaces of Al6061 matrix alloy and Al6061–9 wt% composite at different conditions: **a** as-cast Al6061 matrix, **b** as-cast Al6061–9 wt% B_4C, **c** as-rolled Al6061 matrix, **d** as-rolled Al6061–9 wt% B_4C, **e** Al6061 matrix after 5ARB, **f** Al6061–9 wt% B_4C after five ARB, **g–j** the fractured surfaces after aging treatment, respectively

can be attributed to the formation of fine-grained microstructure with rolling process. Since matrix phase boundaries are the main sites of crack initiation, the number of cracks increases with grain refinement so that the size of each facet decrease with rolling (compare Fig. 13a and c). But after rolling of as-cast Al6061–9 wt% B_4C composite, the fractured surface shows a combination of ductile and cleavage features. Also, the fraction of ductile features increase and the size of dimples decrease compared with as-cast condition (compare Fig. 13b and d). Since the particle/matrix interfaces are the preferred sites for nucleation of voids, this phenomenon can be attributed to more uniform distribution of reinforcement particles and elimination of agglomerates compared to as-cast condition. Similar observations are made for Al6061 matrix and AL6061–9 wt % B_4C composite after five ARB cycles (Fig. 13e and f). Figure 13g–j shows the fractured surfaces after aging treatment. It is concluded that the fraction of ductile fracture increases with aging treatment (for example comparing Fig. 13c and g). This can be attributed to the static recrystallization of matrix phase during solution treatment and the formation of dispersed Mg_2Si precipitates at grain boundaries during aging.

4 Conclusions

In the present study, Al6061–B_4C metal matrix composites were fabricated by using stir casting, post-ARB processing and aging treatment. Microstructure and mechanical properties of processed composites were investigated. The main results are as follows:

1. Post-processing with accumulative roll bonding increases the uniformity of the particle's distribution in microstructure. The particle-free zones and agglomerates were decreased with ARB cycles and disappeared at higher strains.
2. The ductility and tensile strength of as stir-casted composites were improved with accumulative roll bonding. This was due to the grain refinement of matrix material and the improvement of particle–matrix bonding strength and also elimination of micropores produced during solidification.
3. Elongation of fabricated composites was increased with the increase in ARB cycles at the initial stages of deformation and then decreased. The increase in elongation could be attributed to the improvement in the bonding strength between the matrix and reinforcing particles and elimination of porosities. The final decrease in elongation was due to work hardening of matrix material and increasing the dislocation density.
4. Hardness of Al6061–B_4C composites was increased with the enhancement of the ARB cycles as well as reinforcement volume fraction.
5. Porosity content of composites decreased with the increase in ARB cycles as a result of particle clusters elimination.
6. Both the elongation to failure and tensile strength were increased with aging treatment. The main reason was the static recrystallization of matrix during solutionizing and a uniform distribution of Mg_2Si precipitates in matrix phase and grain boundaries.

References

1. Saito Y, Utsunomiya H, Tsuji N, Sakai T, *Acta Mater* **47** (1999) 579.
2. Yu H L, Lu C, Tieu A K, Kong C, *Mater Manuf Process* **29** (2014) 448.
3. Takata N, Lee S H, Lim C Y, Kim S S, Tsuji N, *J Nanosci Nanotechnol* **7** (2007) 3985.
4. Jamaati R, Toroghinejad M R, Edris H, *Mater Sci Eng A* **478** (2013) 191.
5. Perez-Prado M T, Valle D, Ruano O A, *Scripta Mater* **51** (2004) 1093.
6. Lee S H, Saito Y, Sakai T, Utsunomiya H, *Mater Sci Eng A* **325** (2002) 228.
7. Pirgazi H, Akbarzadeh A, Petrov R, Kestens L, *Mater Sci Eng A* **497** (2008) 132.
8. Alizadeh M, Paydar M H, *Mater Sci Eng A* **538** (2012) 14.
9. Ahmadi A, Toroghinejad M R, Najafizadeh A, *Mater Des* **53** (2014) 13.
10. Jamaati R, Toroghinejad M R, Dutkiewicz J, Szpunar J A, *Mater Des* **35** (2012) 37.
11. Rezayat M, Akbarzadeh A, Owhadi A, *Compos A Appl Sci Manuf* **43** (2012) 261.
12. Alizadeh M, Paydar M H, *J Alloys Compd* **492** (2010) 231.
13. Torralba J M, Da Costa C E, Velasco F, *J Mater Process Technol* **133** (2003) 203.
14. Chen R, Iwabuchi A, Shimizu T, *Wear* **238** (2000) 110.
15. Cocen U, Onel K, *Compos Sci Technol* **62** (2002) 275.
16. Alizadeh M, Paydar M H, Jazi F S, *Compos B Eng* **44** (2013) 339.
17. Jamaati R, Toroghinejad M R, *Mater Sci Eng A* **527** (2010) 4146.
18. Askarpour M, Sadeghian Z, Reihanian M, *Mater Sci Eng A* **677** (2016) 400.
19. Darmiani E, Danaee I, Golzr M R, Toroghinejad M R, Ashrafi A, Ahmadi A, *Mater Des* **50** (2013) 497.
20. Thuault A, Marinel S, Savary E, Heuguet R, Saunier S, Goeuriot D, Agrawal D, *Ceram Int* **39** (2013) 1215.
21. Kim K H, Chae J H, Park J S, Ahn J P, Shim K B, *Ceram Process Res* **10** (2009) 716.
22. Toptan F, Kilicarslan A, Kerti I, *Mater Sci Forum* **636–637** (2010) 192.
23. Zhang Z, Fortin K, Charette A, *Effect of Titanium on Microstructure and Fluidity of Al–B_4C Composities* (Vol. 46). Springer, Berlin (2011), p 3177.
24. Mahallawy N, Taha M A, Jarfors A, Fredriksson H, *J Alloys Compd* **292** (1999) 221.
25. Emamy* M, Mahta M, Rasizadeh J, *Compos Sci Technol* **66** (2006) 1063.

26. Toptan F, Kilicarslan A, Karaaslan A, Cigdem M, Kerti I, *Mater Des* **31** (2010) 587.
27. Min G, Lee J M, Kang S B, Kim H W, *Mater Lett* **60** (2006) 3255.
28. Khabushan J K, Bonab S B, *Open J Metals* **7** (2017) 9.
29. Fattahalhosseini A, Naseri M, Alemi M H, *J Manuf Process* **22** (2016) 120.
30. Jamaati R, Toroghinejad M R, *Mater Des* **31** (2010) 4816.
31. Auradi V, Rajesh G L, Kori S A, *Proc Mater Sci* **6** (2014) 1068.
32. Amirkhanlou S, Niroumand B, *Mater Des* **32** (2011) 1895.
33. Yu L I, Qiu-lin L I, Dong L I, Wei L I U, Guo-gang S H U, *Trans Nonferrous Metal Soc China* **26** (2016) 2304.